Available online at www.sciencedirect.com

SciVerse ScienceDirect

CERAMICS INTERNATIONAL

Ceramics International 39 (2013) S563–S568

www.elsevier.com/locate/ceramint

Sonochemical synthesis, photocatalysis and photonic properties of 3% Ce-doped ZnO nanoneedles

Oranuch Yayapao[a], Somchai Thongtem[a,d,*], Anukorn Phuruangrat[b,**], Titipun Thongtem[c,d]

[a]Department of Physics and Materials Science, Faculty of Science, Chiang Mai University, Chiang Mai 50200, Thailand
[b]Department of Materials Science and Technology, Faculty of Science, Prince of Songkla University, Hat Yai, Songkhla 90112, Thailand
[c]Department of Chemistry, Faculty of Science, Chiang Mai University, Chiang Mai 50200, Thailand
[d]Materials Science Research Center, Faculty of Science, Chiang Mai University, Chiang Mai 50200, Thailand

Available online 24 October 2012

Abstract

ZnO nanostructured particles doped with 0–3% Ce were successfully synthesized by an ultrasonic solution method. Phase and morphology characterized by XRD, FTIR, SEM, TEM, HRTEM, SAED and EDX revealed the presence of hexagonal wurtzite ZnO nanoneedles with E_{2H} vibration at 426 cm^{-1}, composing of the corresponding elements and growing in the [0 0 1] direction. The 3% Ce-doped ZnO nanoneedles showed the 3.00 eV direct energy gap and 392.6 nm emission by UV–visible absorption and photoluminescence (PL) spectroscopy, including the most effective photocatalytic activity in the solution containing methylene blue.

Keywords: B. Electron microscopy; B. Spectroscopy; B. X-ray methods; E. Functional applications

1. Introduction

The II–VI semiconductors doped with rare-earth (RE) metals are very important for the present technology. They are promising for use as optoelectronic and luminescent devices: fluorescent lamps, cathode ray tube (CRT) phosphors and image intensifiers for X-ray screens [1]. RE atoms possessing special 4f shells are known as excellent candidates for luminescence centers of doped materials due to the transition of intra-4f or 4f–5d narrow emission line. The transitions play important roles in the absorption of RE atoms in the UV range. An energy transfer process from excited semiconductor host to doping lanthanide atoms promoted the doped nanocrystals to circumvent absorption of optically centers with remarkable improvement of luminescent properties [2,3].

Wurtzite ZnO (3.37 eV energy gap and 60 meV exciton binding energy at room temperature) is high electrochemical stability and non toxicity *n*-type oxide [2,4–7]. It is one of the most dominant UV-activated photocatalysts for air and water treatment due to its high photosensitivity and oxidation potential, and low cost. Lanthanide-doped ZnO nanocrystals are one of new classes of luminescent materials for advanced display and lighting applications [1,2]. Thus ZnO is a promising candidate for treatment of environmental pollution, solving the problem of energy depletion and suitably doped with luminescence centers.

In this research, we succeeded in doping Ce into wurtzite ZnO by sonochemistry. Phase, morphologies, UV–visible absorption and photoluminescence were studied, including the investigation of photocatalytic property of Ce-doped ZnO under the UV light.

2. Experimental details

To prepare 0–3% Ce-doped ZnO, 0.005 mol $Zn(NO_3)_2 \cdot 6H_2O$ and 0–3 mol% $Ce(NO_3)_3 \cdot 6H_2O$ were dissolved into 100 ml deionized water under vigorous stirring till complete dissolution. Subsequently, NH_4OH solution was slowly dropped into these solutions until the pH reaching at 9.5 and colorless solutions were achieved. Each of colorless solutions was sonicated in 35 kHz ultrasonic bath for 5 h.

*Corresponding author at: Chiang Mai University, Department of Physics and Materials Science, Faculty of Science, Chiang Mai 50200, Thailand. Tel.: +66 53 941924; fax: +66 53 943445.
**Corresponding author. Tel.: +66 74 288374; fax: +66 74 288395.
E-mail addresses: schthongtem@yahoo.com (S. Thongtem), phuruangrat@hotmail.com (A. Phuruangrat).

0272-8842/$ - see front matter
http://dx.doi.org/10.1016/j.ceramint.2012.10.136

The precipitates were synthesized and collected for further characterization.

The photocatalytic activities of the as-synthesized samples were determined by measuring the degradation of methylene blue (MB) solution under UV light irradiation. The 500 mg photocatalyst was added to 100 ml 10^{-5} M MB aqueous solution. The solution was magnetically stirred for 60 min in the dark environment to establish adsorption/desorption equilibrium of MB on surfaces of the photocatalyst. Then the UV light was turned on to initiate the photocatalytic reaction.

3. Results and discussion

Fig. 1(a) shows XRD spectra of Ce-doped ZnO with different Ce^{3+} contents. For pure ZnO, the peaks were at 2θ of 32.11, 34.75, 36.59, 47.85 and 56.93 degree corresponding to the (1 0 0), (0 0 2), (1 0 1), (1 0 2) and (1 1 0) planes of hexagonal wurtzite ZnO of the JCPDS No. 36-1451 [8]. By doping Ce^{3+} in ZnO, only the ZnO peaks were still detected. No diffraction peaks of doping atoms or other phases were detected, indicating that the Ce^{3+} ions completely substituted for Zn^{2+} ions in ZnO

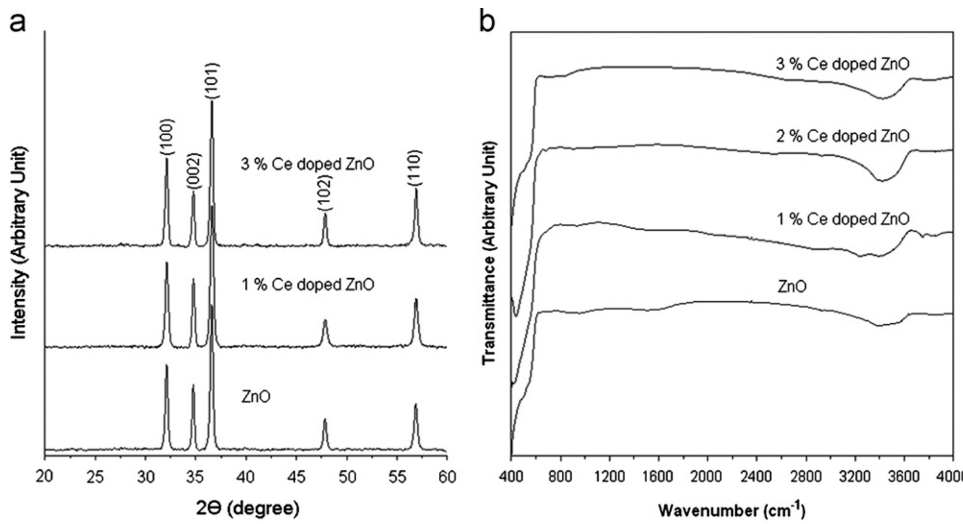

Fig. 1. (a) XRD and (b) FTIR spectra of ZnO with and without Ce doping.

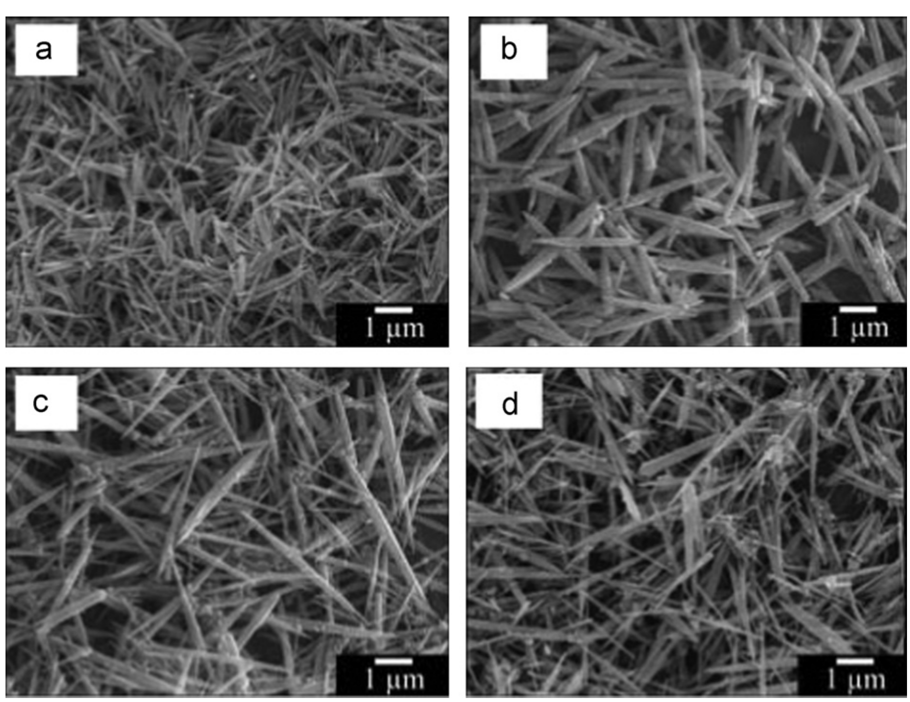

Fig. 2. SEM images of (a) undoped ZnO, and ((b)–(d)) 1, 2 and 3% Ce-doped ZnO, respectively.

lattice. Ce^{3+} concentration could be too low to be detected by XRD.

FTIR spectra (Fig. 1(b)) of the 0–3% Ce-doped ZnO, analyzed over the wave number of 400–4000 cm^{-1}, show strong bands at around 450–500 cm^{-1} with one broad band at 3300–3600 cm^{-1}. In this research, pure ZnO and 1–3% Ce-doped ZnO show the same strong absorption bands at 426 cm^{-1} with the shoulders at 565 cm^{-1}, assigned as E_{2H}

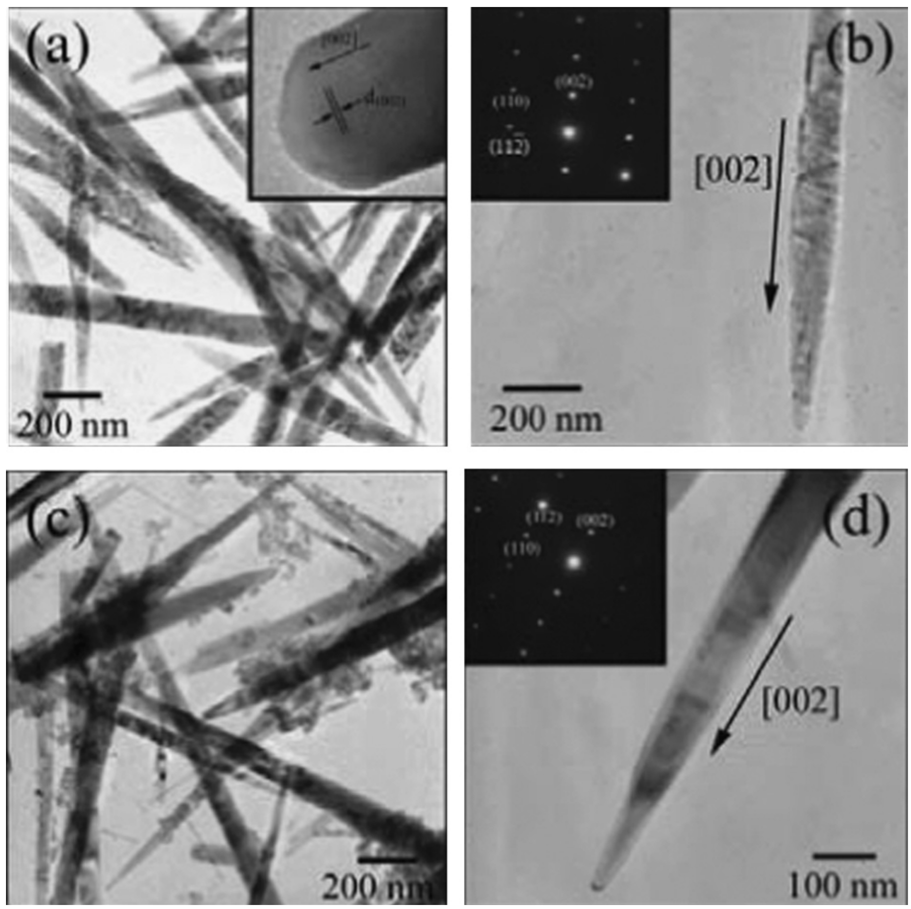

Fig. 3. TEM images, HRTEM images and SAED patterns of (a) and (b) pure ZnO and (c) and (d) 3% Ce-doped ZnO.

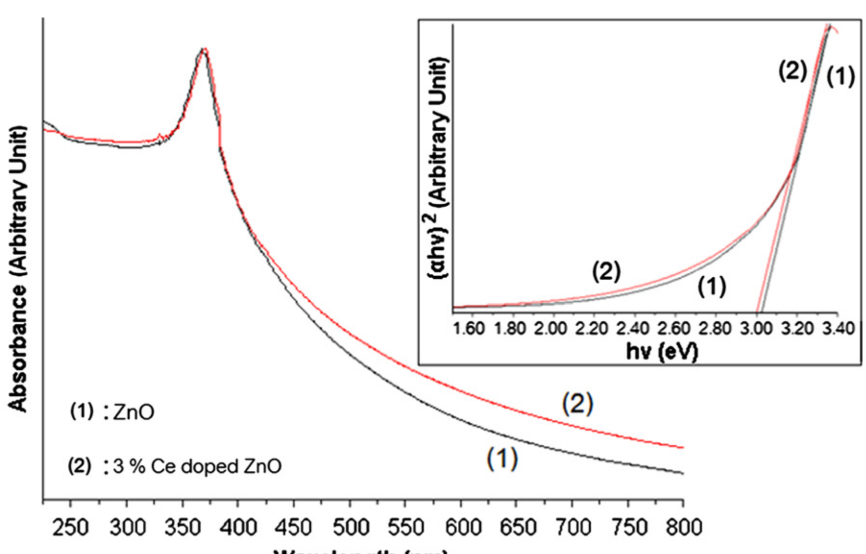

Fig. 4. UV–visible absorption and the $(\alpha h\nu)^2$ vs $h\nu$ plots of ZnO and 3% Ce-doped ZnO.

vibration and oxygen vacancies of wurtzite ZnO crystal, respectively [9]. For every two Ce^{3+} ions doped into ZnO crystal, one O^{2-} vacancy formed to maintain electroneutrality of the crystal. Considering the ionic radii of Zn^{2+} and Ce^{3+} [6,10,11], it was likely that Ce^{3+} partially substituted for Zn^{2+} in the ZnO crystal. An absorption bands at 3300–3600 cm^{-1} is the O–H stretching of adsorbed water on the sample surface.

Pure ZnO (Fig. 2(a)) was nanoneedle-like particles with sharp tips on both ends. A base width at the middle and tapered tips were 100 nm and 25 nm with 1 μm long. By doping with Ce (Fig. 2(b)–(d)), the morphology of 1–3% Ce-doped ZnO remained as nanoneedles, but their lengths were increased to 2–3 μm. The elemental distribution of 3% Ce-doped ZnO nanoneedles were characterized by EDX. Zn, O and Ce were shown on the elemental EDX-maps (result not shown), implying that Ce atoms were very distributive in the sample.

TEM and HRTEM images and SAED pattern (Fig. 3(a) and (b)) represent phase and morphology of pure ZnO nanoneedles with 800 nm long, uniform diameter and slightly rough surface. The HRTEM image was analyzed on edge part of a typical ZnO nanoneedle. The (0 0 2) fringe at right angle to the [0 0 1] growth direction with 2.61 Å apart were detected, in consistent with that of the bulk wurtzite ZnO crystal. Some defects were also detected. The SAED pattern shows a bright spot pattern of single crystal of hexagonal ZnO. Consider the 3% Ce-doped ZnO images and SAED pattern (Fig. 3(c) and (d)), they revealed the straight nanoneedles of single crystal with smooth surface and 80 nm in diameter. The *d*-spacing values measured from the SAED pattern with zone axis of [1–10] are 1.62 Å, 1.38 Å and 2.61 Å, well agree with the (1 1 0), (1 1 2) and (0 0 2) lattice planes of hexagonal ZnO phase, respectively. These indicated that 3% Ce-doped ZnO nanoneedles grew along the [0 0 1] direction.

Formation mechanism of ZnO nanoneedles proceeded in a sonochemical bath as follows. First, zinc nitrate, water and ammonium hydroxide absorbed ultrasound energy and followed by the dissociation process to form primary ions. Second, $[Zn(OH)_4]^{2-}$ complex ions formed and further decomposed to give ZnO molecules [12], which nucleated and grew as nanoneedles. Their preferential growth were along the [0 0 0 1] direction due to the intrinsic anisotropy in growth rate (v) with v[0 0 0 1] > v[0 1-1 0] > v[0 0 0 -1]. The structure of ZnO single crystal can be described as a number of alternating planes of coordinated Zn^{2+} and O^{2-} ions, the positively charged Zn-(0 0 0 1) and negatively charged O-(0 0 0 1) polar surfaces. Due to the decreasing in the concentration of ZnO_2^{2-} monomers by the rapid nucleation of ZnO, the absorption of OH^- on the positively charged plane dominated the competition of ZnO_2^{2-} growth units. Thus, the OH^- ions stabilized the surface charge of Zn-(0 0 0 1) to some degree, leading to the formation of nanoneedle-like ZnO along the [0 0 0 1] direction [13,14]. When the doping material was also mixed, Ce^{3+} ions diffused and resided in the ZnO nanoneedles.

UV absorption (Fig. 4) of undoped ZnO and 3% Ce-doped ZnO was investigated in 225–800 nm wavelength range. They presented well defined excitonic absorption peaks at 366 nm, corresponding to the band-to-band

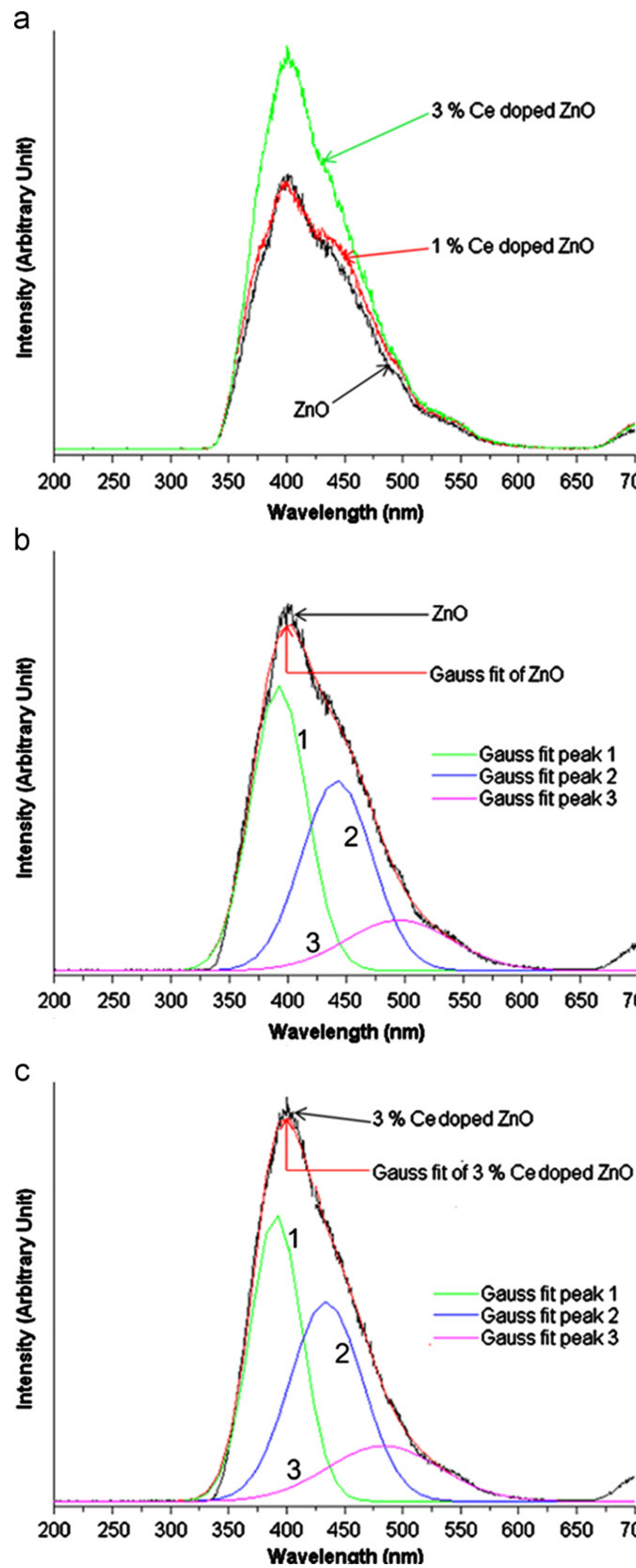

Fig. 5. (a) PL spectra of ZnO with and without Ce doping. Gaussian analysis of (b) ZnO and (c) 3% Ce-doped ZnO.

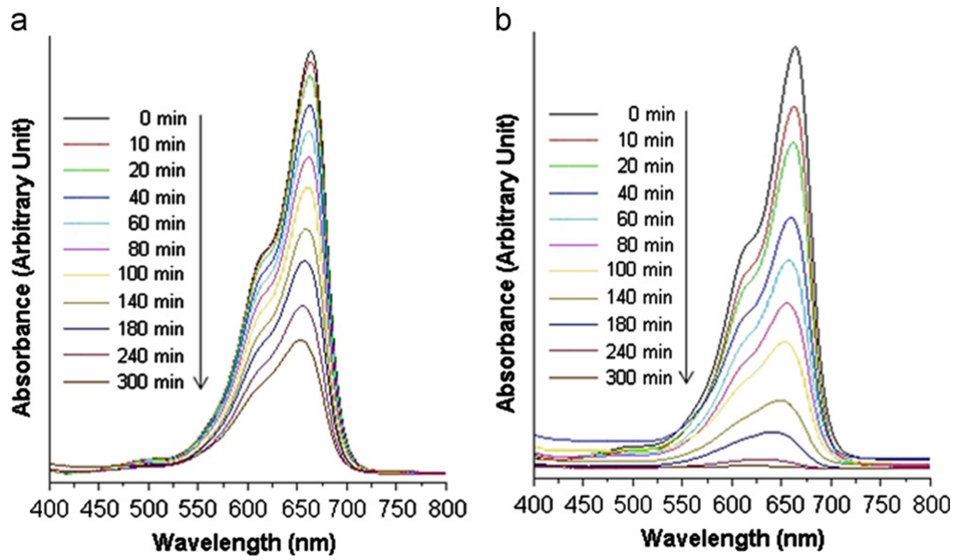

Fig. 6. UV–visible absorption of (a) pure ZnO and (b) 3% Ce-doped ZnO.

transition of ZnO [15], and at 370 nm of 3% Ce-doped ZnO with red shifted absorption as compared to that for ZnO. The direct energy gaps of undoped ZnO and 3% Ce-doped ZnO were determined to be 3.03 and 3.00 eV, respectively.

PL spectra (Fig. 5) of ZnO with and without Ce doping were studied using 318 nm excitation wavelength. They showed broad emissions in the wavelength range of 325–600 nm. The 3% Ce-doped ZnO showed higher emission intensity than any other products. Upon doing the Gaussian analysis for pure ZnO and 3% Ce-doped ZnO with the highest intensity, the spectra were disintegrated into three emission peaks at 393.1 nm, 442.9 nm and 495.6 nm for pure ZnO, and 392.6 nm, 433.7 nm and 482.2 nm for 3% Ce-doped ZnO-corresponding to the UV, blue and blue-green emissions, respectively [16,17]. The first was caused by the characteristic of near-band-edge emission of free exciton recombination process [18], but the second and third were possibly associated with oxygen vacancies [16] and other defects.

MB is adopted as a representative organic pollutant to evaluate the photocatalytic performance of the as-synthesized Ce-doped ZnO. UV–visible absorbance (Fig. 6) of undoped ZnO and 3% Ce-doped ZnO during photocatalysis for 0–300 min shows that the absorbance of MB for ZnO was gradually decreased, but that for 3% Ce-doped ZnO was decreased at much faster rate. Fig. 7 shows the MB degradation rate for ZnO with and without Ce doping under UV light for different lengths of time. Obviously, 3% Ce-doped ZnO shows the most effective in photocatalysis in these solutions. During the first 140 min, MB concentration was rapidly decreased to 32, 70 and 87% for ZnO, 1% Ce-doped ZnO and 3% Ce-doped ZnO, respectively. For 240 min, the MB degradation efficiency for 3% Ce-doped ZnO was higher than 98%, 1.97 times the degradation efficiency of ZnO (49.81%). The higher

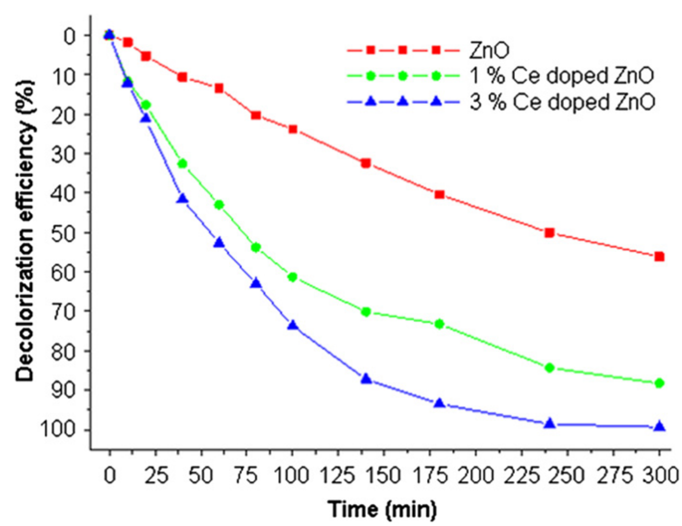

Fig. 7. Decolorization efficiencies of ZnO with and without Ce doping.

the concentration of oxygen defects on the surfaces of Ce-doped ZnO nanocrystals is, the stronger the photocatalytic activity will be. Finally, the experimental results presented in this article will be very useful for the research on other metallic/semiconducting catalysts with high catalytic activities.

4. Conclusions

Undoped ZnO and 1–3% Ce-doped ZnO nanoneedles were successfully synthesized in a controlled sonochemical process. The PL spectrum of 3% Ce-doped ZnO showed a strong emission at 392.6 nm with other two weak visible emissions. The facile, reproducible and effective route presented a useful method for the RE^{3+}-doped ZnO system. High crystalline quality and good optical properties of the

Ce-doped ZnO nanoneedles can lead the material to be a candidate for different applications in the future.

Acknowledgements

We wish to thank the Thailand Research Fund for financial support through the research grant BRG5380020, and the Thailand's Office of the Higher Education Commission through the National Research University Project for Chiang Mai University (CMU), including the Graduate School of CMU through the general support.

References

[1] J. Iqbal, X. Liu, H. Zhu, Z.B. Wu, Y. Zhang, D. Yu, R. Yu, Raman and highly ultraviolet red-shifted near band-edge properties of LaCe-co-doped ZnO nanoparticles, Acta Materialia 57 (2009) 4790–4796.

[2] Y.P. Du, Y.W. Zhang, L.D. Sun, C.H. Yan, Efficient energy transfer in monodisperse Eu-doped ZnO nanocrystals synthesized from metal acetylacetonates in high-boiling solvents, The Journal of Physical Chemistry C 112 (2008) 12234–12241.

[3] J. Flor, S.A.M. de Lima, M.R. Davolos, Effect of reaction time on the particle size of ZnO and ZnO:Ce obtained by a sol–gel method, Progress in Colloid and Polymer Science 128 (2004) 239–243.

[4] H.C. Gong, J.F. Zhong, S.M. Zhou, B. Zhang, Z.H. Li, Z.L. Du, Ce-induced single-crystalline hierarchical zinc oxide nanobrushes, Superlattices and Microstructures 44 (2008) 183–190.

[5] Z. Sofiani, B. Derkowska, P. Dalasiński, M. Wojdyła, S. Dabos-Seignon, M. Alaoui Lamrani, L. Dghoughi, W. Bała, M. Addou, B. Sahraoui, Optical properties of ZnO and ZnO:Ce layers grown by spray pyrolysis, Optics Communications 267 (2006) 433–439.

[6] D. Fangli, W. Ning, Z. Dongmei, S. Yingzhong, Preparation, characterization and infrared emissivity study of Ce-doped ZnO films, Journal of Rare Earths 28 (2010) 391–395.

[7] Y. Morinaga, K. Sakuragi, N. Fujimura, T. Ito, Effect of Ce doping on the growth of ZnO thin films, Journal of Crystal Growth 174 (1997) 691–695.

[8] Powder Diffract. File, JCPDS-ICDD, 12 Campus Boulevard, Newtown Square, PA 19073-3273, U.S.A. (2001).

[9] G. Xiong, U. Pal, J.G. Serrano, K.B. Ucer, R.T. Williams, Photoluminescence and FTIR study of ZnO nanoparticles: the impurity and defect perspective, Physica Status Solidi C Current Topics in Solid State Physics 3 (2006) 3577–3581.

[10] C. Ge, C. Xie, S. Cai, Preparation and gas-sensing properties of Ce-doped ZnO thin-film sensors by dip-coating, Materials Science and Engineering B 137 (2007) 53–58.

[11] J.E. Huheey, E.A. Keiter, R.L. Keiter, Inorganic Chemistry.: Principles of Structure and Reactivity, fourth ed., Harper Collins College Publ., NY 10022, U.S.A, 1993.

[12] P. Mishra, R.S. Yadav, A.C. Pandey, Growth mechanism and photoluminescence property of flower-like ZnO nanostructures synthesized by starch-assisted sonochemical method, Ultrasonics Sonochemistry 17 (2010) 560–565.

[13] B. Li, Y. Wang, Facile synthesis and enhanced photocatalytic performance of flower-like ZnO hierarchical microstructures, The Journal of Physical Chemistry C 114 (2010) 890–896.

[14] D. Wang, C. Song, Controllable synthesis of ZnO nanorod and prism arrays in a large area, The Journal of Physical Chemistry B 109 (2005) 12697–12700.

[15] H. Qin, W. Li, Y. Xia, T. He, Photocatalytic activity of heterostructures based on ZnO and N-doped ZnO, ACS Applied Materials & Interfaces 3 (2011) 3152–3156.

[16] Z. Zhu, D. Yang, H. Liu, Microwave-assisted hydrothermal synthesis of ZnO rod-assembled microspheres and their photocatalytic performances, Advanced Powder Technology 22 (2011) 493–497.

[17] C. Deng, H. Hu, G. Shao, C. Han, Facile template-free sonochemical fabrication of hollow ZnO spherical structures, Materials Letters 64 (2010) 852–855.

[18] J. Das, D. Khushalani, Nonhydrolytic route for synthesis of ZnO and its use as a recyclable photocatalyst, The Journal of Physical Chemistry C 114 (2010) 2544–2550.